

Supporting Information

Mechanistic Understanding of the Interfacial Properties of Metal-PtSe₂ Contacts

*Luijian Qi, Mengqi Che, Mingxiu Liu, Bin Wang, Nan Zhang, Yuting Zou, Xiaojuan Sun,
Zhiming Shi, Dabing Li and Shaojuan Li**

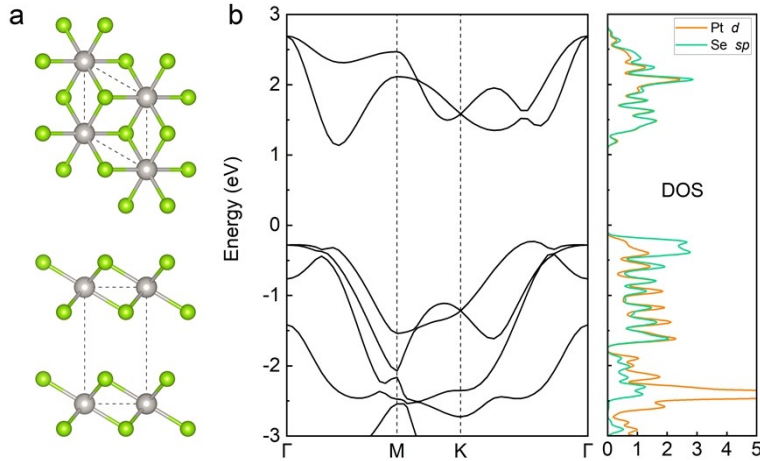


Figure S1. (a) Atomic structures of bulk PtSe₂ with 1T phase. (b) Band structures and density of states of monolayer PtSe₂.

Table S1. Total energy (eV) of possible stacking configurations for metal-PtSe₂ contacts.

| Energy (eV) | Type I | Type II | Type III |
|----------------------|------------------|------------------|------------------|
| Ag-PtSe ₂ | -189.7475 | -189.7505 | -189.7764 |
| Al-PtSe ₂ | -220.0505 | -220.0588 | -220.0629 |
| Au-PtSe ₂ | -217.4000 | -217.3996 | -217.3914 |
| Cu-PtSe ₂ | -215.8513 | -215.9233 | - |
| Pd-PtSe ₂ | -295.8074 | -295.8145 | -295.9051 |
| Pt-PtSe ₂ | -338.2266 | -338.2190 | -338.2775 |
| Sc-PtSe ₂ | -197.7589 | -197.8269 | - |
| Ti-PtSe ₂ | -395.1130 | -395.2772 | -395.1684 |

Table S2. The structural parameters (\AA) of the metal-PtSe₂ contacts. The values in parentheses represent the structural parameters of the metal-BL PtSe₂ contacts.

| | Ag | Al | Au | Cu | Pd | Pt | Sc | Ti |
|----------------------|----------------|----------------|----------------|----------------|----------------|----------------|----------------|----------------|
| lattice constants | 7.59 (7.59) | 7.56 (7.56) | 7.58 (7.58) | 6.65 (6.65) | 7.41 (7.41) | 7.44 (7.44) | 6.57 (6.57) | 7.67 (7.67) |
| interlayer distances | 2.49 (2.46) | 2.42 (2.37) | 2.58 (2.55) | 2.19 (2.17) | 2.17 (2.15) | 2.26 (2.34) | 2.13 (2.11) | 2.07 (2.03) |

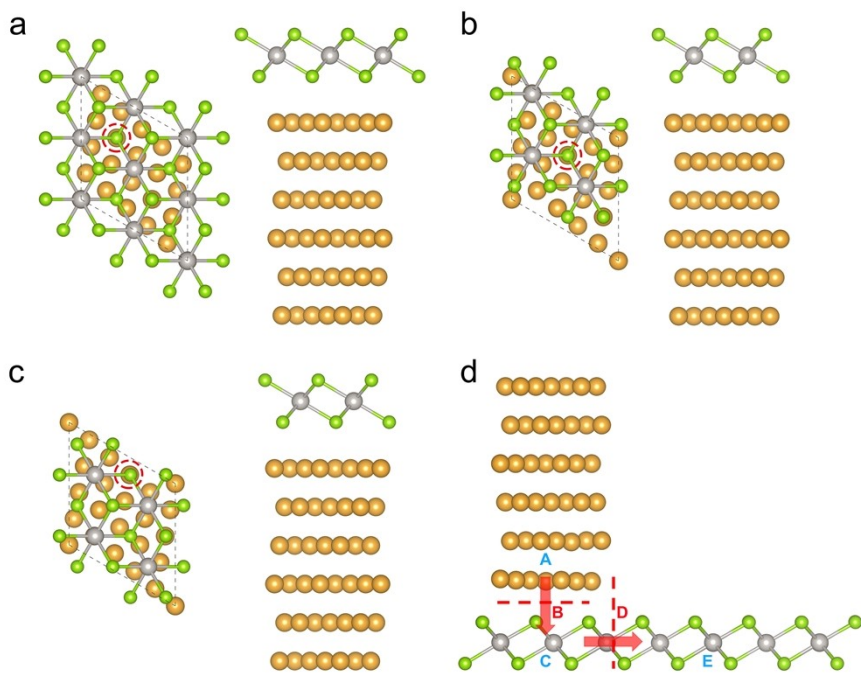


Figure S2. (a)-(c) Three different high symmetric stacking configurations of Au-PtSe₂ contacts. The red dotted circles in (a)-(c) represent the FCC hollow site, HCP hollow site and top site for the Se atom in the circle, respectively. (d) Schematic view of metal-PtSe₂ contacts. A, C, and E denote the metal, PtSe₂ at the region of contact and channel, respectively. B and D are the vertical and lateral interface, respectively. Red arrows represent the pathway of electron injection from metal to PtSe₂ channel.

Table S3. Binding energy E_b (J/m²) of metal-PtSe₂ contacts.

| | Ag | Al | Au | Cu | Pd | Pt | Sc | Ti |
|------------|------|------|------|------|------|------|------|------|
| E_b (ML) | 1.27 | 0.97 | 1.23 | 1.82 | 2.08 | 2.00 | 2.25 | 2.61 |
| E_b (BL) | 1.36 | 1.07 | 1.31 | 1.94 | 2.22 | 2.15 | 2.43 | 2.83 |

Table S4. Binding energy E_b (eV) of Ag, Al, Au, Cu, Pd, Pt, Sc and Ti based metal-monolayer PtSe₂ contacts. Here, the binding energy are calculated as: $E_b = (E_{\text{metal}} + E_{\text{PtSe}_2} - E_{\text{heterostructure}})/N$ for comparison with previous studies.

| E_b | Ag | Al | Au | Cu | Pd | Pt | Sc | Ti | Ref |
|-------------------------|-------|-------|-------|-------|-------|-------|-------|-------|--------------------|
| PtSe₂ | -0.99 | -0.75 | -0.96 | -1.45 | -1.55 | -1.50 | -1.75 | -2.08 | Our results |
| MoS ₂ | -0.27 | -0.24 | -0.20 | - | -0.69 | -0.48 | - | - | [1] |
| MoS ₂ | -0.50 | - | -0.31 | - | - | -0.57 | -1.18 | -1.81 | [2] |
| MoSe ₂ | -0.13 | -0.04 | - | - | - | -0.29 | - | -0.71 | [3] |
| WS ₂ | -0.62 | - | -0.28 | -0.76 | - | -0.82 | -1.27 | -1.08 | [4] |
| WSe ₂ | -0.30 | -0.29 | -1.18 | - | -0.60 | -0.53 | -0.92 | - | [5] |

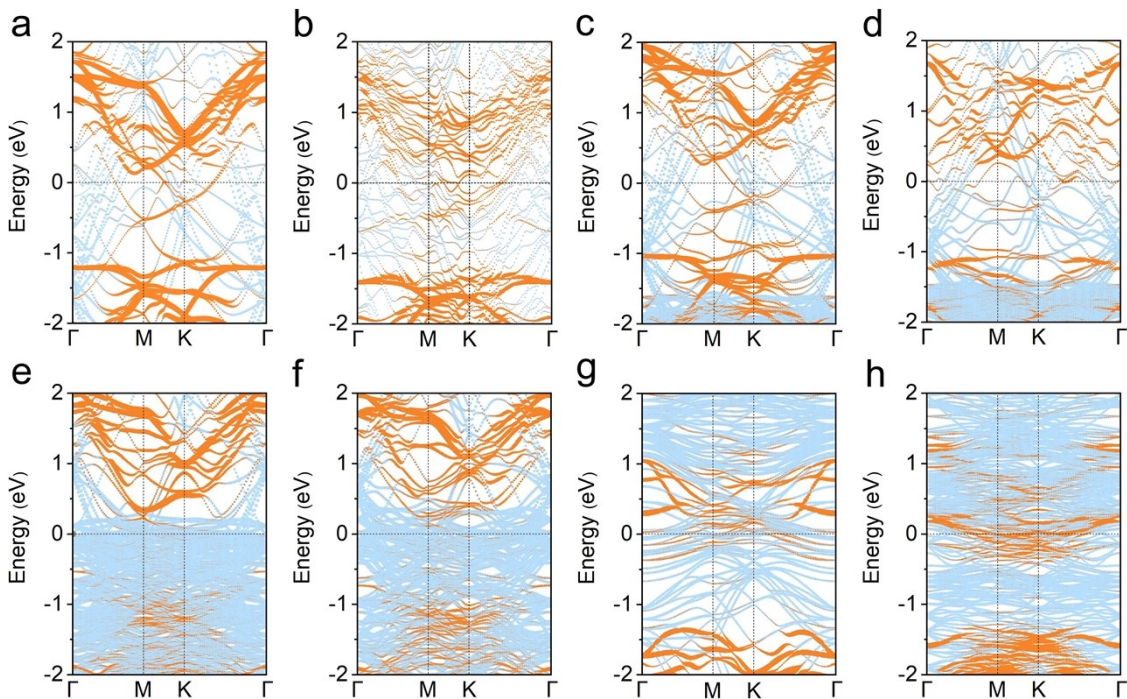


Figure S3. The projected band structures of Ag, Al, Au, Cu, Pd, Pt, Sc and Ti based metal-monolayer PtSe₂ contacts in (a)-(h). Orange and bule colors represent the contributions from PtSe₂ and metal, respectively.

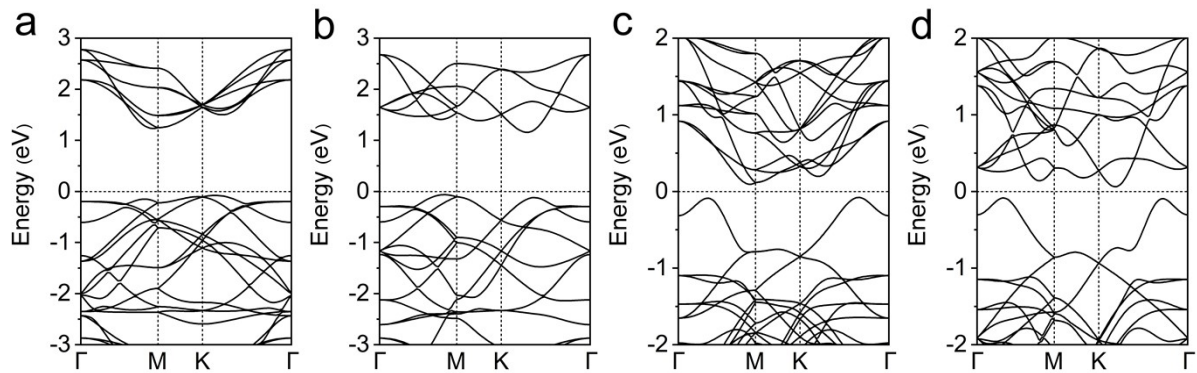


Figure S4. The band structures of original supercell PtSe₂ in metal-PtSe₂ contacts. (a) and (c) represent the cases of ML and BL PtSe₂ with Ag, Al, Au, Pd, Pt and Ti, respectively. (b) and (d) represent the cases of ML and BL PtSe₂ with Cu and Ti, respectively.

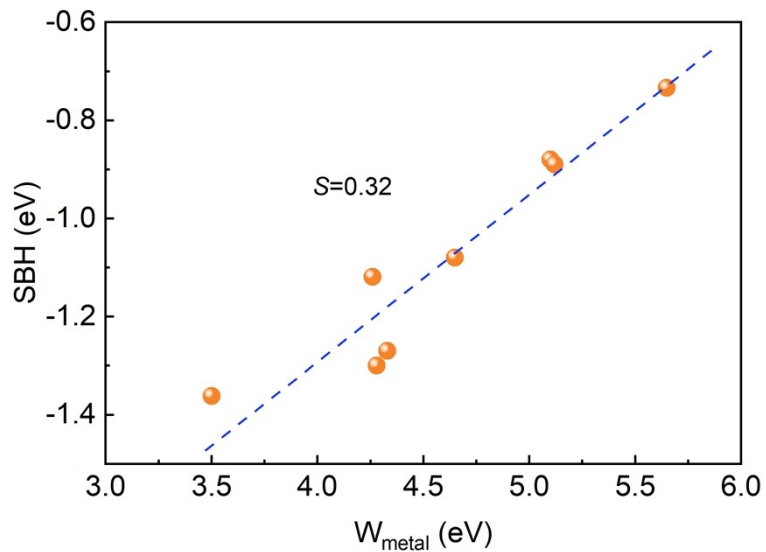


Figure S5. The fitting of FLP factor for Ag, Al, Au, Cu, Pd, Pt, Sc and Ti based metal-monolayer PtSe₂ contacts.

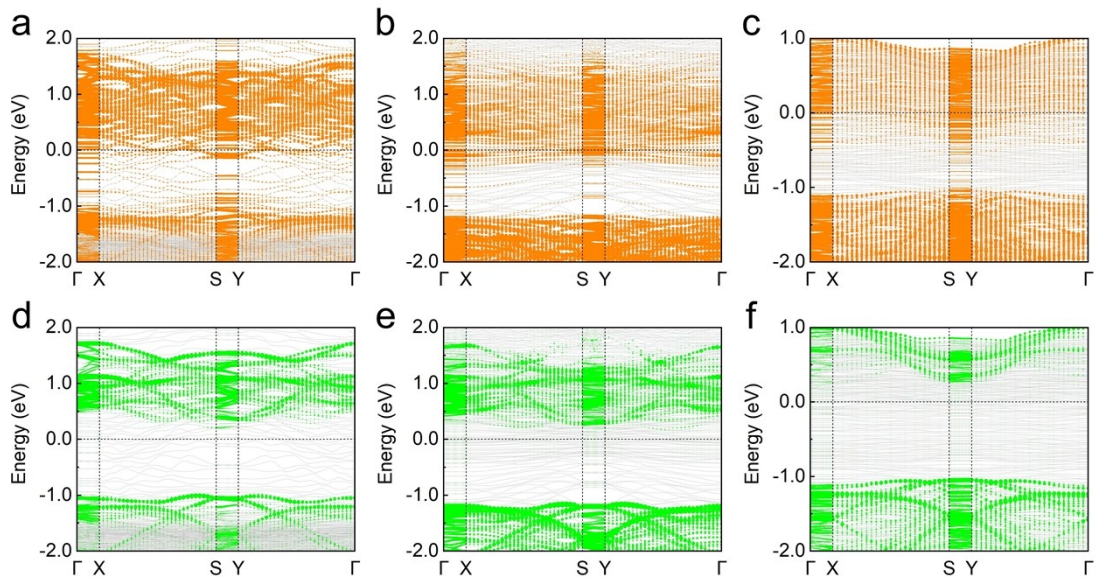


Figure S6. Band structure of PtSe_2 in the large supercell model at the vertical metal contact region (indicated by orange) and the lateral free-standing PtSe_2 region (indicated by green) for Cu ((a) and (d)), Sc ((b) and (e)) and Ti ((c) and (f)) based systems. (noting that the Fermi level is same in the corresponding systems, respectively)

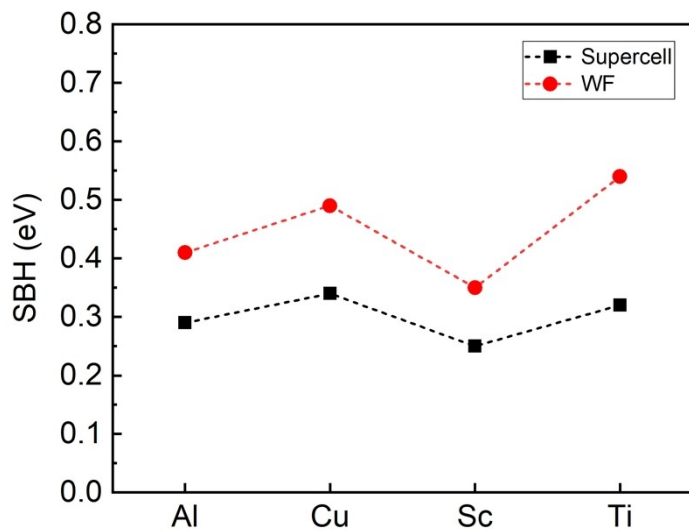


Figure S7. Schottky barrier height of the metal- PtSe_2 systems based on the work function approximation and large supercell model.

Table S5. The actual distance d (\AA) between metal atoms and interfacial Se atoms as well as the covalent distance (sum of the covalent radii of metal atom and Se atom).

| | Ag | Al | Au | Cu | Pd | Pt | Sc | Ti |
|-------------------|------|------|------|------|------|------|------|------|
| d | 2.85 | 2.78 | 3.06 | 2.58 | 2.53 | 2.59 | 2.75 | 2.64 |
| | 2.84 | 2.77 | 2.66 | 2.56 | 2.53 | 2.58 | 2.70 | 2.47 |
| | 2.82 | 2.75 | 2.66 | 2.33 | 2.52 | 2.58 | 2.56 | 2.47 |
| | 2.58 | 2.51 | 2.66 | - | 2.35 | 2.37 | - | 2.47 |
| shortest d | 2.58 | 2.51 | 2.66 | 2.33 | 2.35 | 2.37 | 2.56 | 2.47 |
| average d | 2.77 | 2.70 | 2.76 | 2.49 | 2.48 | 2.53 | 2.67 | 2.51 |
| covalent distance | 2.50 | 2.34 | 2.50 | 2.33 | 2.44 | 2.46 | 2.60 | 2.48 |

Table S6. The tunneling barrier and tunneling probability for the case of van der Waals interlayer distance (3.5\AA) between metal and PtSe_2 in metal- PtSe_2 contacts.

| vdW distance | ΔV | Δd | TB |
|--------------|------------|------------|-------|
| Au | 4.37 | 1.78 | 2.21% |
| Cu | 4.13 | 1.88 | 2.00% |
| Sc | 3.14 | 1.58 | 5.69% |
| Ti | 3.60 | 1.66 | 3.97% |

Table S7. Tunneling barrier height Φ_{TB} (eV), width d_{TB} (\AA), tunneling probability (%) and tunneling-specific resistivity ($\Omega \text{ cm}^2$) of metal-monolayer PtSe₂ contacts.

| | Φ_{TB} | d_{TB} | Probability | Resistivity |
|----|--------------------|-----------------|-------------|-------------|
| Ag | 1.69 | 0.71 | 38.63 | 3.00E-11 |
| Al | 0.93 | 0.50 | 61.04 | 1.80E-11 |
| Au | 2.22 | 0.80 | 29.38 | 3.86E-11 |
| Cu | 0.69 | 0.38 | 72.65 | 1.33E-11 |
| Pd | 0.79 | 0.33 | 74.08 | 1.06E-11 |
| Pt | 0.98 | 0.39 | 67.47 | 1.23E-11 |
| Sc | 0.00 | 0.00 | 100.00 | 0 |
| Ti | 0.00 | 0.00 | 100.00 | 0 |

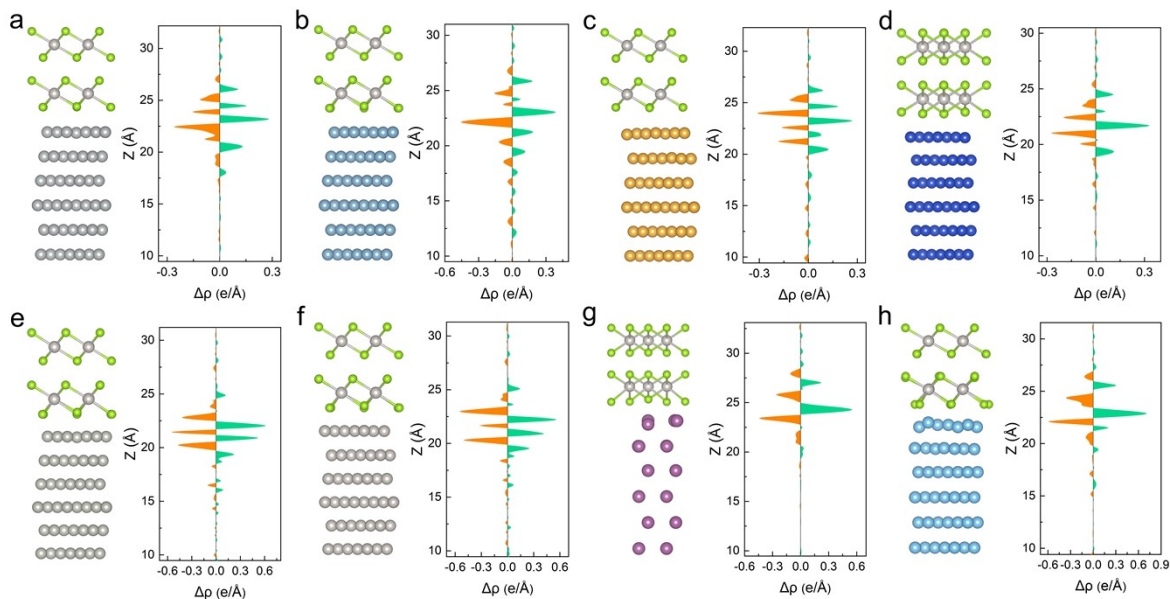


Figure S8. Side view of the optimized atomic structures and plane charge density differences for Ag, Al, Au, Cu, Pd, Pt, Sc and Ti based metal-bilayer PtSe₂ contacts in (a)-(h), respectively.

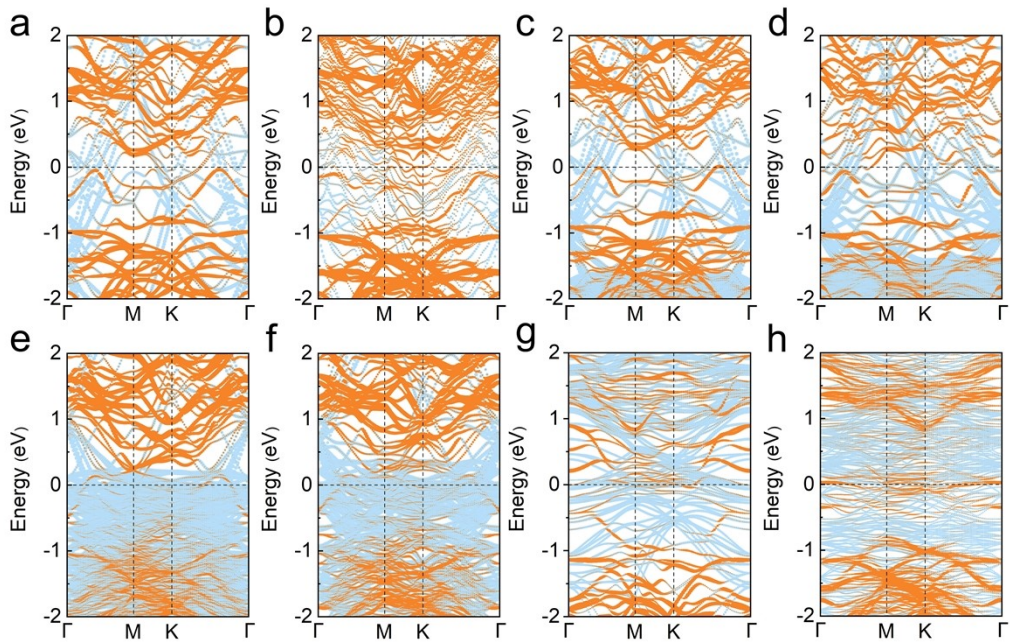


Figure S9. Projected band structures of Ag, Al, Au, Cu, Pd, Pt, Sc and Ti based metal-bilayer PtSe₂ contacts in (a)-(h).

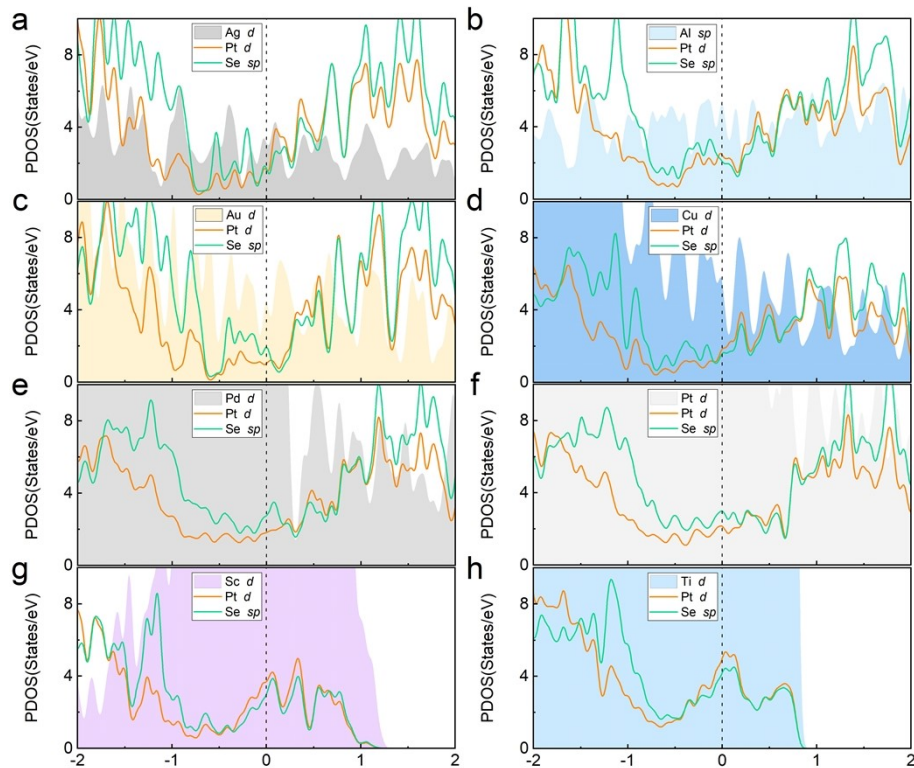


Figure S10. Partial density of states for PtSe₂ and metal in Ag, Al, Au, Cu, Pd, Pt, Sc and Ti based metal-bilayer PtSe₂ contacts in (a)-(h).

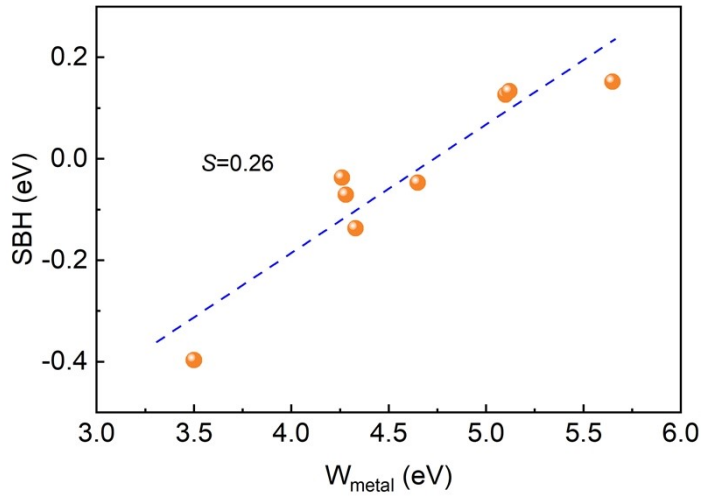


Figure S11. The fitting of FLP factor for Ag, Al, Au, Cu, Pd, Pt, Sc and Ti based metal-bilayer PtSe₂ contacts.

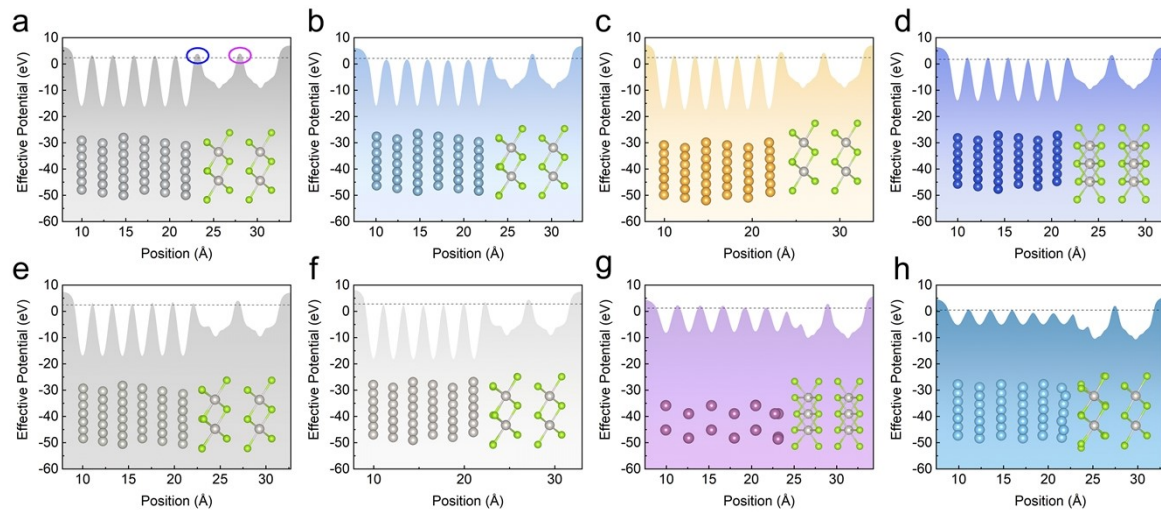


Figure S12. Effective potential along the vertical position for Ag, Al, Au, Cu, Pd, Pt, Sc and Ti based metal-bilayer PtSe₂ contacts in (a)-(h).

Table S8. Tunneling barrier height Φ_{TB} (eV), width d_{TB} (\AA), tunneling probability (%) and tunneling-specific resistivity ($\Omega \text{ cm}^2$) of the interface between metal and first-layer PtSe₂ and the interface between the first-layer and second-layer in metal-monolayer PtSe₂ contacts.

| | Metal-PtSe ₂ | | | | First layer PtSe ₂ -Second layer PtSe ₂ | | | |
|-------------------|-------------------------|-----------------|-------------|-------------|---|-----------------|-------------|-------------|
| | Φ_{TB} | d_{TB} | Probability | Resistivity | Φ_{TB} | d_{TB} | Probability | Resistivity |
| Ag | 1.571 | 0.667 | 42.48 | 2.64E-11 | 1.647 | 0.649 | 42.62 | 2.50E-11 |
| Al | 0.697 | 0.416 | 70.07 | 1.50E-11 | 1.744 | 0.674 | 40.19 | 2.68E-11 |
| Au | 2.166 | 0.785 | 30.63 | 3.67E-11 | 1.763 | 0.682 | 39.56 | 2.74E-11 |
| Cu | 0.629 | 0.353 | 75.08 | 1.25E-11 | 1.685 | 0.628 | 43.40 | 2.35E-11 |
| Pd | 0.706 | 0.299 | 77.32 | 0.97E-11 | 1.650 | 0.659 | 42.03 | 2.58E-11 |
| Pt | 0.852 | 0.348 | 71.97 | 1.11E-11 | 1.678 | 0.666 | 41.34 | 2.62E-11 |
| Sc | 0.000 | 0.000 | 100.00 | 0 | 1.646 | 0.63 | 43.71 | 2.37E-11 |
| Ti | 0.000 | 0.000 | 100.00 | 0 | 1.571 | 0.601 | 46.24 | 2.19E-11 |
| PtSe ₂ | - | - | - | - | 0.976 | 0.389 | 40.33 | 2.67E-11 |

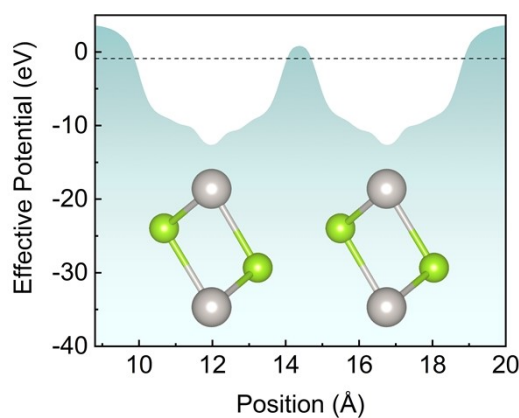


Figure S13. Effective potential along the vertical direction for bilayer PtSe₂. The dotted line represents the Fermi energy level.

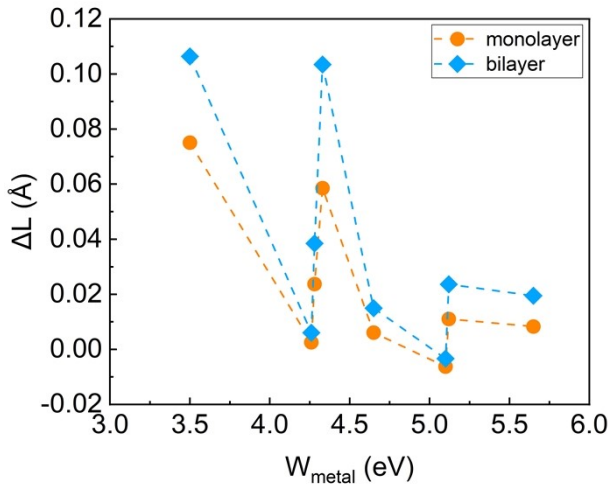


Figure S14. The change of the average bond length of the interfacial Se atom and Pt atom in PtSe_2 versus the work function of metals.

Table S9. The lattice parameters a (\AA) and interfacial distance (\AA) of metal-BN-PtSe₂ contacts.

| | Ag | Al | Au | Pd | Pt | Ti |
|---------------------------|------|------|------|------|------|------|
| a | 7.59 | 7.56 | 7.58 | 7.41 | 7.44 | 7.67 |
| $d_{\text{Metal-BN}}$ | 3.16 | 3.57 | 3.23 | 2.97 | 3.16 | 2.18 |
| $d_{\text{BN-PtSe}_2}$ | 3.36 | 3.38 | 3.34 | 3.35 | 3.34 | 3.28 |
| $d_{\text{Metal-PtSe}_2}$ | 6.52 | 6.95 | 6.57 | 6.32 | 6.50 | 5.46 |

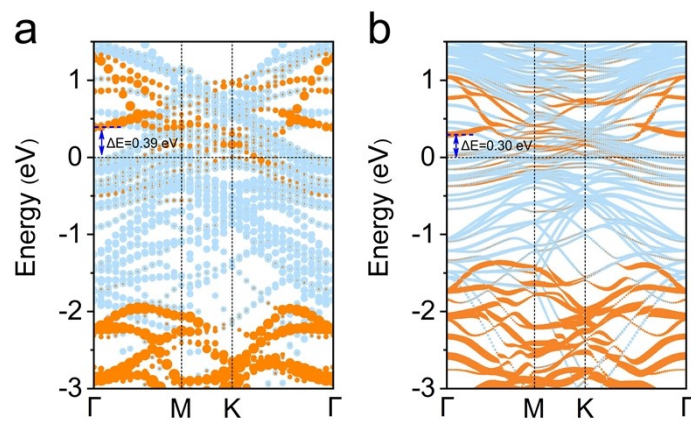


Figure S15. Comparison of the HSE06-based band structure (a) and the PBE-based band structure (b) of Sc-PtSe₂ contact. ΔE represents the energy difference between the Fermi level energy and one major conduction band of PtSe₂.

Table S10. The lattice mismatch and introduced strain for Metal-PtSe₂ contacts.

| | Ag | Al | Au | Cu | Pd | Pt | Sc | Ti |
|--------------|------|------|------|------|-------|-------|------|------|
| Mismatch (%) | 1.41 | 0.48 | 1.06 | 3.51 | 3.56 | 2.67 | 1.31 | 3.46 |
| Strain (%) | 0.71 | 0.24 | 0.53 | 1.79 | -1.75 | -1.32 | 0.66 | 1.76 |

References

- (1) Gong, C.; Colombo, L.; Wallace, R. M.; Cho, K. The unusual mechanism of partial Fermi level pinning at metal-MoS₂ interfaces. *Nano Lett.* **2014**, *14* (4), 1714.
- (2) Zhong, H.; Quhe, R.; Wang, Y.; Ni, Z.; Ye, M.; Song, Z.; Pan, Y.; Yang, J.; Yang, L.; Lei, M. et al. Interfacial properties of monolayer and bilayer MoS₂ contacts with metals: beyond the energy band calculations. *Sci. Rep.* **2016**, *6*, 21786.
- (3) Pan, Y.; Li, S.; Ye, M.; Quhe, R.; Song, Z.; Wang, Y.; Zheng, J.; Pan, F.; Guo, W.; Yang, J. et al. Interfacial properties of monolayer MoSe₂–metal contacts. *J. Phys. Chem. C* **2016**, *120* (24), 13063.
- (4) Tang, H.; Shi, B.; Pan, Y.; Li, J.; Zhang, X.; Yan, J.; Liu, S.; Yang, J.; Xu, L.; Yang, J. et al. Schottky contact in monolayer WS₂ field-effect transistors. *Adv. Theor. Simul.* **2019**, *2* (5), 1900001.
- (5) Wang, Y.; Yang, R. X.; Quhe, R.; Zhong, H.; Cong, L.; Ye, M.; Ni, Z.; Song, Z.; Yang, J.; Shi, J. et al. Does p-type ohmic contact exist in WSe₂-metal interfaces? *Nanoscale* **2016**, *8* (2), 1179.